Simulation of elastic moduli for porous materials

Charles P. Ursenbach

ABSTRACT

A simulation method is employed to simulate elastic moduli of porous materials, including error estimation. The ratio of porous elastic moduli to their non-porous counterparts is obtained for isotropic skeletal materials with a Poisson's ratio of ¼. Three cases are modeled: 1). The spherical pores are non-overlapping but otherwise randomly distributed spheres, 2) the spherical pores are randomly distributed (overlapping) spheres, and 3) the pores are exclusions created from randomly distributed, overlapping spheres of matrix material. In all cases the pores are empty and the spheres are uniform in size. The results show that Norris' differential effective medium theory describes overlapping spheres well, particularly compressional properties, and the Kuster-Toksöz model is moderately accurate for non-overlapping spheres. The CPA gives the closest description of the spherical exclusions, but it is still poor.

INTRODUCTION

A fundamental problem in processing reservoir data is understanding how elastic properties vary with porosity, as such information provides input to the Biot-Gassmann theories. A variety of theories have been developed to address this problem. The Kuster-Toksöz (Kuster, 1974) method based on scattering theory assumes that pores are dilute and non-overlapping. The differential effective medium (DEM) theory can also describe non-overlapping pores (Zimmerman, 1984) or overlapping pores (Norris, 1985). The simplest form of these theories is obtained for the case of spherical pores in isotropic media, and these have been reviewed by Zimmerman (1991). The CPA theory (Berryman, 1992) treats pores and matrix symmetrically, and in that sense is more likely to apply to spherical exclusions.

Comparison of various theories against experiment can be found in Berge *et al.* (1993) and Zimmerman (1991). In these studies, glass foam (with a bulk glass Poisson's ratio of $\sigma = 0.23$) is treated as having uniform spherical pores. Berge *et al.* find that the compressional velocity (V_P) of glass foam is intermediate between the Kuster-Toksöz model [equivalent in this case to the Hashin model (Hashin, 1962)] and Norris' DEM [although comparison with Zimmerman's DEM would be more appropriate, as glass foam consists of non-overlapping pores (Walsh, 1965)]. Zimmerman finds similar results for the normalized bulk modulus. Berge et al. also studied fused glass beads, which are more similar to spherical exclusions (but non-overlapping) and found them to be well described by the CPA theory.

Such results are as those above are useful, but suffer from the drawback that one is dealing with errors both from theoretical approximations as well as from the incongruence of real substances with ideal pore models. Simulation is very helpful in this regard, as it allows one to assess theoretical results directly against pseudo-experimental data for the idealized pore models, with only well-controlled errors

resulting from the simulation. Thus the purpose of this study is to carry out assessment of theory analogous to the above references (Berge, 1993; Zimmerman, 1991) but using simulation data instead of experimental data.

Such simulation methods, while not yet widely used in the rock physics community, are not new either. A number of workers in composite materials have carried out simulations of matter with spherical inclusions using a variety of simulation models, such as a point mass and spring lattice model (Day *et al*., 1992; Snyder *et al.*, 1992), or the more general finite element method (Garboczi & Day, 1995; Chen *et al*., 1995), or boundary element methods (Eischen, 1993; Helsing, 1995; Christiansson, 1996). Indeed, seismic wave propagation problems have also been studied using spring lattice methods (Krebes, 1987; Paranjape *et al.,* 1987; Scales, 2000). In the rock physics realm, Poutet *et al.* (1996) have performed a valuable simulation study on the physics of various pore arrangements. Thus there is a considerable history of application that can be adapted to rock physical problems.

DESCRIPTION OF SIMULATION METHOD

This study employs the point mass and spring lattice simulation model. While not as general as the finite element method, it is very simple and intuitive. Continuum matter is modeled as a collection of point masses connected by springs in a regular lattice. Certain conditions must be placed upon the springs in order for the lattice to model an elastic material. For instance, suppose we are modeling isotropic matter, with a specified density and Lamé's constants, μ and λ. Then displacements in the lattice and the resulting stresses should be related by the following well-known equation:

$$
\begin{bmatrix} \sigma_{11} \\ \sigma_{22} \\ \sigma_{33} \\ \sigma_{12} \\ \sigma_{23} \\ \sigma_{31} \end{bmatrix} = \begin{bmatrix} 2\mu+\lambda & \lambda & \lambda & 0 & 0 & 0 \\ \lambda & 2\mu+\lambda & \lambda & 0 & 0 & 0 \\ \lambda & \lambda & 2\mu+\lambda & 0 & 0 & 0 \\ 0 & 0 & 0 & 2\mu & 0 & 0 \\ 0 & 0 & 0 & 0 & 2\mu & 0 \\ 0 & 0 & 0 & 0 & 0 & 2\mu \end{bmatrix} \begin{bmatrix} \varepsilon_{11} \\ \varepsilon_{22} \\ \varepsilon_{33} \\ \varepsilon_{12} \\ \varepsilon_{23} \\ \varepsilon_{31} \end{bmatrix} \tag{1}
$$

Suppose that we have a simple cubic array of point masses (where each mass is given by the density times the cubic grid element volume). Let nearest neighbours be connected by springs with a force constant of k_1. An analysis of this system reveals that to linear order the stress-strain relation would be

$$\begin{bmatrix} \sigma_{11} \\ \sigma_{22} \\ \sigma_{33} \\ \sigma_{12} \\ \sigma_{23} \\ \sigma_{31} \end{bmatrix} = \frac{1}{dl} \begin{bmatrix} k_1 & 0 & 0 & 0 & 0 & 0 \\ 0 & k_1 & 0 & 0 & 0 & 0 \\ 0 & 0 & k_1 & 0 & 0 & 0 \\ 0 & 0 & 0 & 0 & 0 & 0 \\ 0 & 0 & 0 & 0 & 0 & 0 \\ 0 & 0 & 0 & 0 & 0 & 0 \end{bmatrix} \begin{bmatrix} \varepsilon_{11} \\ \varepsilon_{22} \\ \varepsilon_{33} \\ \varepsilon_{12} \\ \varepsilon_{23} \\ \varepsilon_{31} \end{bmatrix} \tag{2}$$

where *dl* is the nearest neighbour grid distance. This clearly cannot represent elastic material for any value of k_1. Suppose one chooses instead to place springs between next-nearest neighbours (k_2), or next-next-nearest neighbours (k_3). These choices result in

$$\frac{1}{dl} \begin{bmatrix} 2k_2 & k_2 & k_2 & 0 & 0 & 0 \\ k_2 & 2k_2 & k_2 & 0 & 0 & 0 \\ k_2 & k_2 & 2k_2 & 0 & 0 & 0 \\ 0 & 0 & 0 & 2k_2 & 0 & 0 \\ 0 & 0 & 0 & 0 & 2k_2 & 0 \\ 0 & 0 & 0 & 0 & 0 & 2k_2 \end{bmatrix}, \frac{4/3}{dl} \begin{bmatrix} k_3 & k_3 & k_3 & 0 & 0 & 0 \\ k_3 & k_3 & k_3 & 0 & 0 & 0 \\ k_3 & k_3 & k_3 & 0 & 0 & 0 \\ 0 & 0 & 0 & 2k_3 & 0 & 0 \\ 0 & 0 & 0 & 0 & 2k_3 & 0 \\ 0 & 0 & 0 & 0 & 0 & 2k_3 \end{bmatrix} \tag{3}$$

Again, neither of these matrices is consistent with elastic matter. However, by combining any two of the above types of spring one can represent an elastic Poisson solid ($\mu=\lambda$). As pointed out by Krebes (private communication), to obtain the $\mu \neq \lambda$ case requires, for instance, a hinge spring between three masses forming a right angle. This spring would yield a matrix of the form

$$\begin{bmatrix} 0 & 0 & 0 & 0 & 0 & 0 \\ 0 & 0 & 0 & 0 & 0 & 0 \\ 0 & 0 & 0 & 0 & 0 & 0 \\ 0 & 0 & 0 & 2k & 0 & 0 \\ 0 & 0 & 0 & 0 & 2k & 0 \\ 0 & 0 & 0 & 0 & 0 & 2k \end{bmatrix} \tag{4}$$

which can be combined with two of the above spring types to yield a general elastic solid. In this study I have modeled a Poisson solid with k_1 and k_3 springs (this choice minimizes the number of springs).

Various workers (Montroll, 1947; Gazis *et al.*, 1960; Krebes, 1987; Paranjape *et al.*, 1987) have implemented this model using a Lagrangian formulation. In this study it has been implemented by discretizing Newton's second law in a manner analogous to molecular simulation techniques (e.g., Allen and Tildesley, 1987). Periodic boundary conditions are applied. Pore locations are generated from random numbers, and pores are created by eliminating point masses and springs in the pore region.

To calculate the bulk modulus, a small compression is applied by rescaling the location of all point masses from their equilibrium positions. For a porous solid this

results in unbalanced forces on the masses, and their positions are allowed to relax to equilibrium, which generally shrinks the pore regions further. Viscous forces are applied to the masses to approximate critical damping in this process. At equilibrium the bulk modulus is calculated from the change in energy via the relation $\delta E = \frac{1}{2} K (\delta V/V)^2$.

The shear modulus is calculated in a similar manner, except that a volume-preserving distortion is applied instead, such as a shear strain, or a compression in one direction and compensating extension in the others. For a single shear strain the modulus is extracted using $\delta E = \frac{1}{2} \mu \, \varepsilon_{ij}^2$.

SOURCES OF ERROR

For simulation results to be maximally useful, it is critical to produce error bars for the results. Six sources of error were identified in these simulations. Two are trivial, two result from the finite size of the simulation cell, and two from the discrete grid representation.

Trivial sources of error

One source of error arises from the fact that the energy is never fully minimized due to the iterative approach. Appropriate choice of a convergence criterion however ensures that this is not a significant source of error. Similarly, the non-linear dependence of effective stress on strain means that the calculated moduli are, strictly speaking, strain dependent. Choosing a small enough strain however produces a result in the linear domain, so the results are strain independent.

Finite-sample sources of error

In Figure 1 below, a two-dimensional cartoon illustrates that a variety of different configurations are consistent with a given porosity and pore size. Yet they will all have distinct elastic moduli. The true modulus (for this sample size) is obtained by averaging over the moduli of every such configuration possible. This is clearly impossible, and we must be satisfied with a finite number of configurations. This introduces one source of error, which can be expressed quantitatively as the standard deviation of values obtained (which we denote F_W), divided by the square root of the number of configurations.

K_1 K_2 K_3

K_4 K_5 K_6
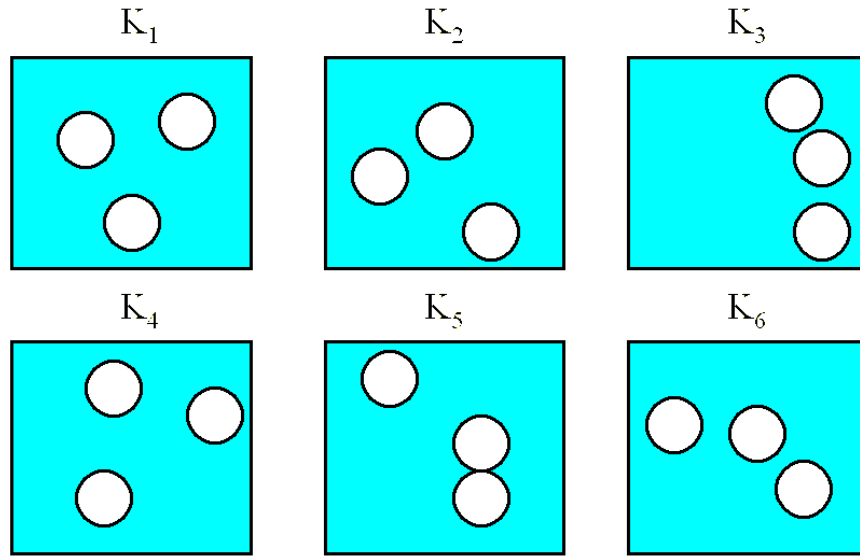
$$K = (1/n)\ \Sigma\ K_i$$

FIG. 1. Schematic two-dimensional representation of various configurations of non-overlapping spherical pores in a simulation cell of fixed size.

Yet even if one could employ an infinite number of configurations, one would still not obtain the correct result. For this one would require an infinitely large simulation cell (or pore sizes infinitesimally smaller than the cell size). This is illustrated in Figure 2 below, where it is clear that averages over all configurations of the two models shown will not give identical results. The error of the average we will denote F_A. (Incidentally, if one had an infinitely large simulation cell, one would also need to generate only one configuration, i.e., F_W divided by the simulation result would approach zero.)
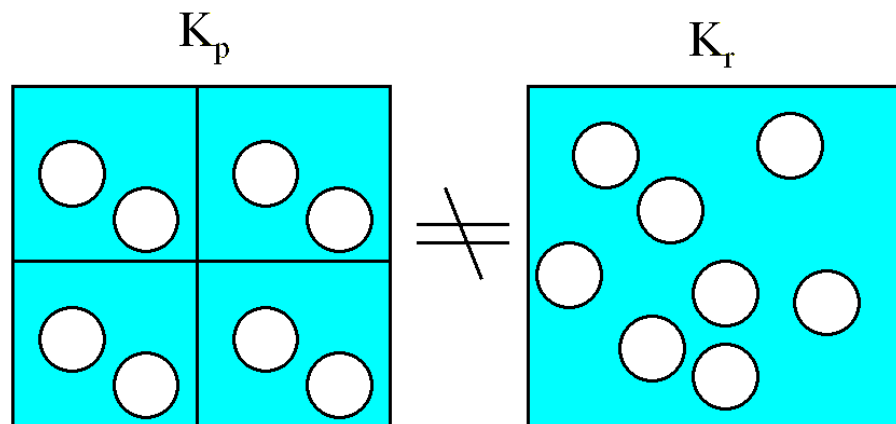
K_p K_r

FIG. 2. A schematic illustrating that the average over configurations in a large simulation cell is not equivalent to the average for a periodically repeated small cell.

Discrete-grid sources of error

The discussion above of finite-sample errors assumes that the energy of any one configuration can be known exactly. However, because the skeletal material is represented by discrete points of matter, arbitrary pore shapes cannot be represented exactly. In fact, because of the periodic boundary conditions, a random translation of any pore configuration should not change the energy for perfectly represented pores, but a grid representation will result in a distribution of values (with standard deviation G_W), as illustrated in Figure 3 below.
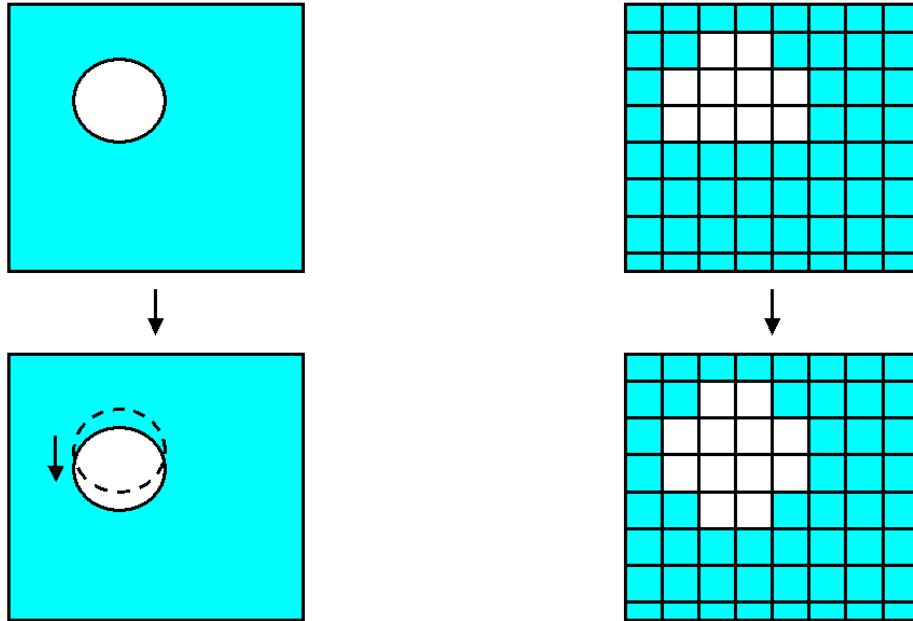
FIG. 3. Schematic illustration of how the translation of a perfectly round pore in a simulation cell can result in a change of shape of the pore when it is represented on a discrete grid.

Supposing then that one averages over all possible translations of a given configuration, one will still obtain a result that depends on grid size. The error of this, compared to the exact value for that configuration, we will denote G_A. As the grid size decreases, as illustrated in Figure 4, the pore description will improve and one will approach a smaller distribution of more correct values.
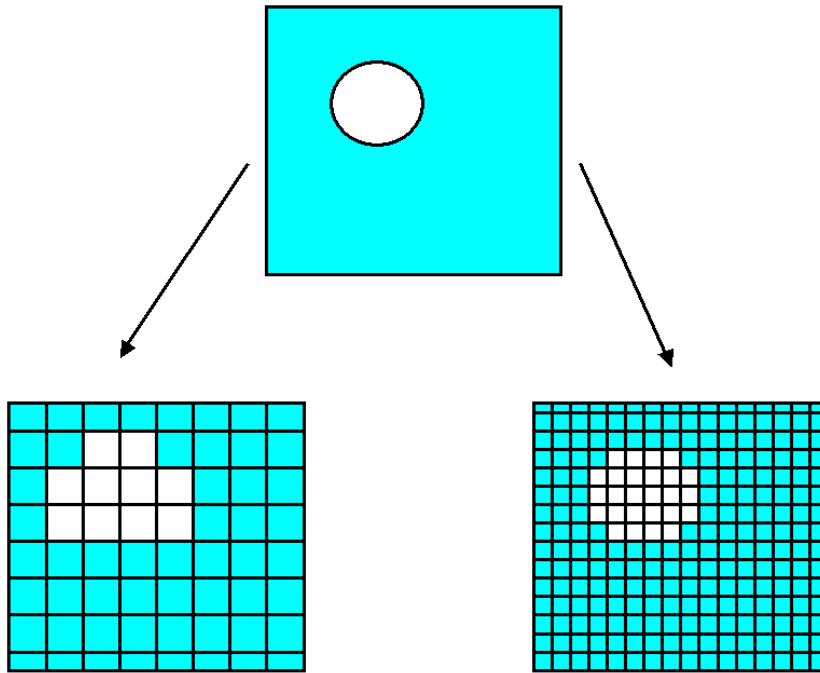
FIG. 4.   A schematic drawing illustrating that finer grids are able to represent arbitrarily shaped pores more accurately than coarse grids.

Combined sources of error

The various concepts above are illustrated in a practical way in Figure 5, which presents results from actual simulations. Each point represents one simulation, and the normalized bulk modulus is plotted against the grid spacing in a cell of fixed size. The crosses represent simulations of a variety of configurations, while the circles represent simulations of one single pore configuration, translated randomly to various locations within the unit cell. It is clear that, for the parameters employed here, the distribution of values for one configuration (G_W) is far smaller than the distribution for an ensemble of configurations (F_W). It is also clear that the distribution due to grid size increases with grid size (empirically, it increases as the square of the grid width), while the configurational distribution is independent of grid size, as expected. Furthermore, values for one configuration vary roughly linearly with grid size, with approximately the same slope for each configuration, so that one can estimate the infinitesimal grid width value, both for individual configurations and for the average.
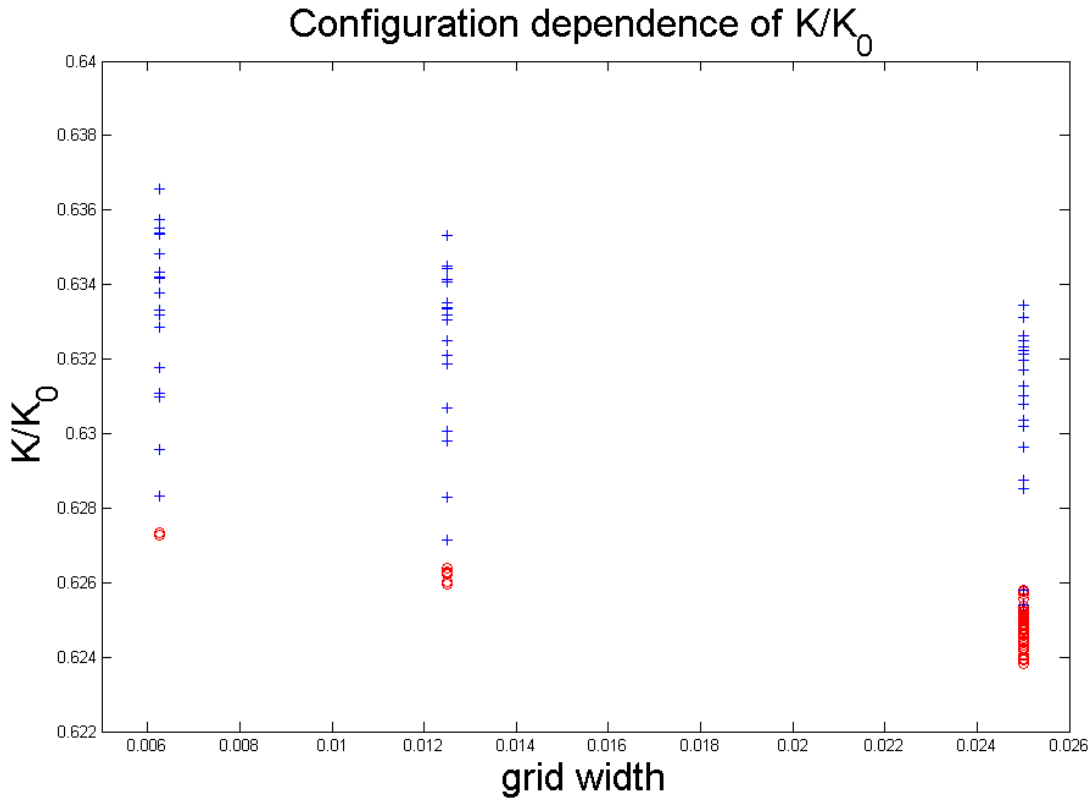
FIG. 5. The result of simulations for non-overlapping spherical pores with $\phi = 0.2$. Each cross represents a different configuration of pores, while all the circles at a given grid width represent one single configuration translated to various locations in the cell. The distribution of crosses is F_W and the distribution of circles is G_W. Note the linear behavior of each configuration that permits approximate extrapolation back to zero grid width.

In the above figure the cell size is fixed and the grid width varies. The opposite case is shown in Figure 6, below which displays results of simulations for various configurations and cell sizes but with fixed porosity, grid width, and pore size. The observed change in F_W with cell size is found empirically to vary as $(r/L)^{3/2}$, where r is a pore dimension (e.g., radius) and L is a cell dimension (e.g., edge length).
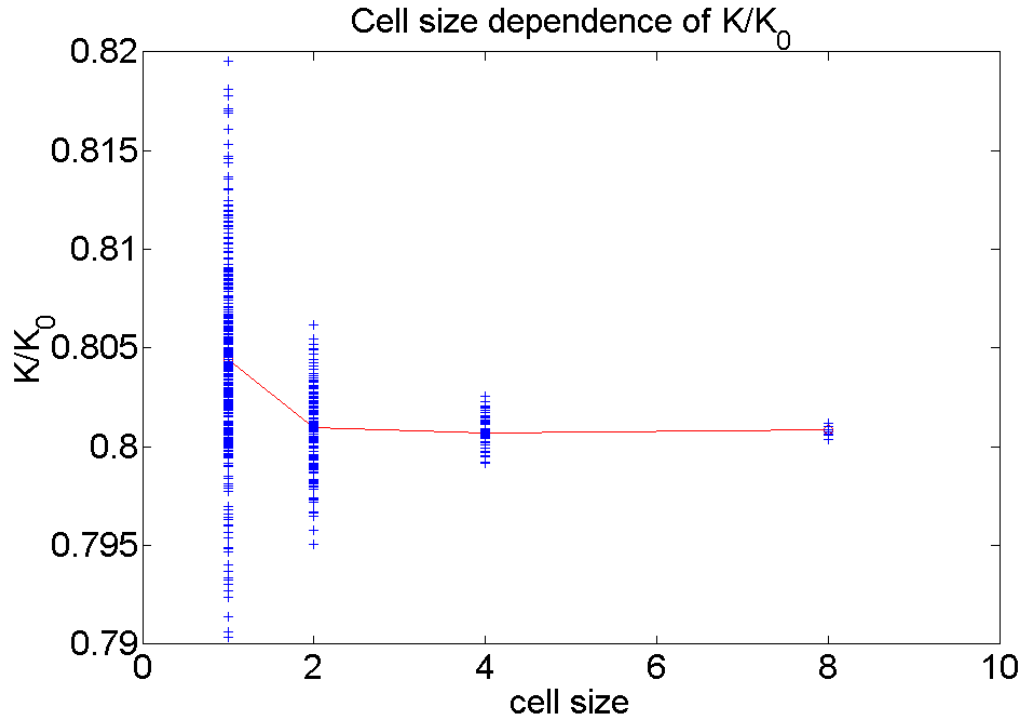
FIG. 6. The result of simulations for non-overlapping spherical pores with $\phi = 0.1$. Each cross represents a different configuration of pores, and the distribution of crosses is F_W. Note that the average value converges rapidly (i.e., $F_A \rightarrow 0$) as the cell dimensions increase relative to the pore dimensions.

A practical approach to error analysis emerges from these figures. First, for suitably small grid widths, $G_W \ll F_W$, and will be ignored. (It is actually subsumed in the latter.) Next, G_A will be approximately removed by linear extrapolation. Finally, from Figure 6 it is appears that for sufficiently small pore:cell ratios, $F_A \ll F_W$. Thus, after the extrapolation procedure, we assume that $F_W /\sqrt{n_{config}}$ is the dominant error (if n_{config} is not too large), and we assign it to be the error for the average of all values at a given porosity.

In some of my earlier work a more approximate approach was used to estimate the error bars. This was employed in the figures below for work on the spherical inclusions, while the above more general method was used for the spherical exclusions. It can be seen below that the present method yields more rigorous error bars.

RESULTS

The spherical pore simulations were carried out on a 160 X 160 X 160 point grid. The spherical exclusion simulations were carried out on both a 160 X 160 X 160 grid ($n_{config} = 3$) and a 80 X 80 X 80 grid ($n_{config} = 60$). Note that computer time varies as N^4 on an N X N X N grid. Typical runs required several hours on a modern Sun Workstation to achieve adequate energy convergence. The simulation samples were compressed by .04% or less in each dimension. The calculated elastic moduli are scaled by their pure bulk values, and are thus independent of the actual values of host

density and moduli. The spheres are in all cases uniform in size, and the pure bulk Poisson's ratio is ¼. The simulation results for bulk and shear moduli (K and μ) are shown in Figures 7and 8 below, normalized by their bulk values. Six other derived quantities are shown in Figures 9 through 14.

The first derived quantity is the λ constant (see Figure 9), obtained as $\lambda = K - (2/3)\,\mu$, or $\lambda/\lambda_0 = (5/3)K/K_0 - (2/3)\,\mu/\mu_0$ (since $K_0/\lambda_0 = 5/3$ and $\mu_0/\lambda_0 = 1$ for the bulk Poisson ratio $\sigma_0 = 1/4$). Thus the propagated error is approximately double that in Figures 7 and 8 [$\Delta(\lambda/\lambda_0) = (5/3)\,\Delta(K/K_0) + (2/3)\,\Delta(\mu/\mu_0)$]. Young's modulus was calculated as well, and is shown in Figure 10. The error bars are quite large for the spherical inclusions. Poisson's ratio was calculated but the propagated error is too large for the results to be useful, and they are not shown. (A more appropriate approach to obtain E and σ would be by a simulation method which constrains ε_{11} while allowing $\varepsilon_{22} = \varepsilon_{33}$ to relax to a minimum energy state). We can also obtain the P-velocity modulus, $\rho V_P^2 / \rho_0 V_{P,0}^2 = (2/3)(\mu/\mu_0) + (1/3)(\lambda/\lambda_0)$, the error of which is similar to that of K and μ (see Figure 11). This quantity could also have been obtained directly from a simulation using $\varepsilon_{22} = \varepsilon_{33} = \varepsilon_{12} = \varepsilon_{13} = \varepsilon_{23} = 0$, whereas λ, E, and σ cannot be obtained directly from this simulation method.

Noting that ρ/ρ_0 is equal to $1 - \phi$, and that $\mu = \rho V_S^2$, we can also calculate $V_P/V_{P,0}$ and $V_S/V_{S,0}$ and their associated errors, as shown in Figures 12 and 13 below.
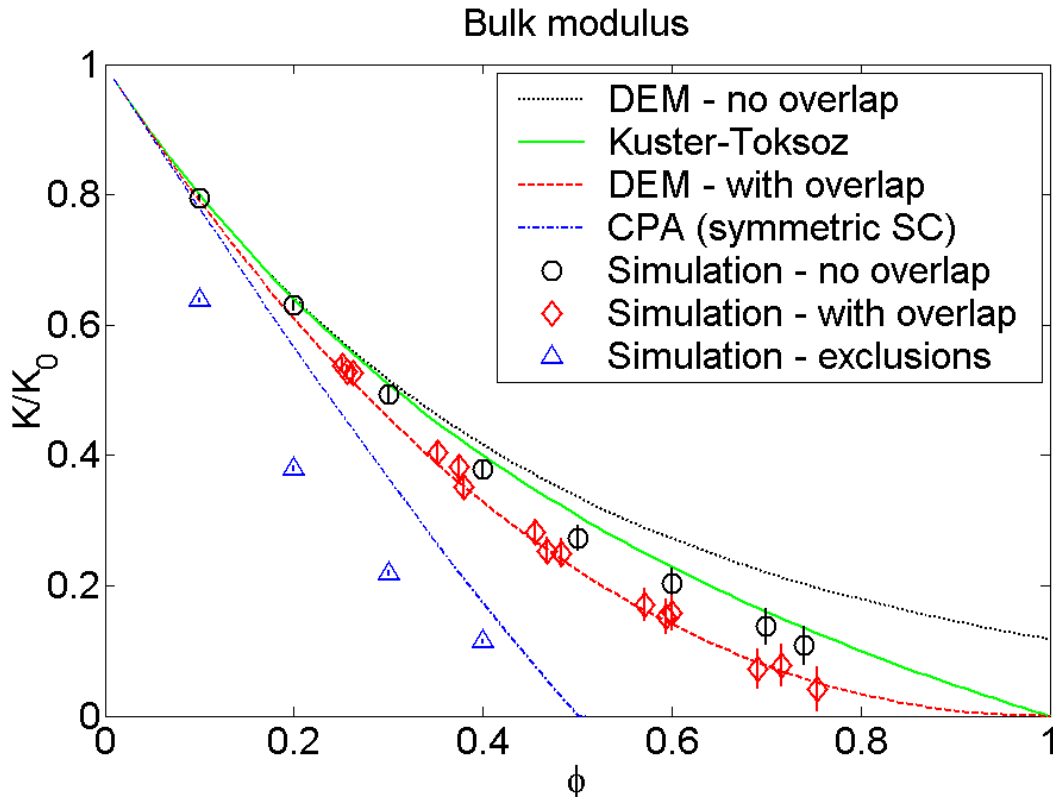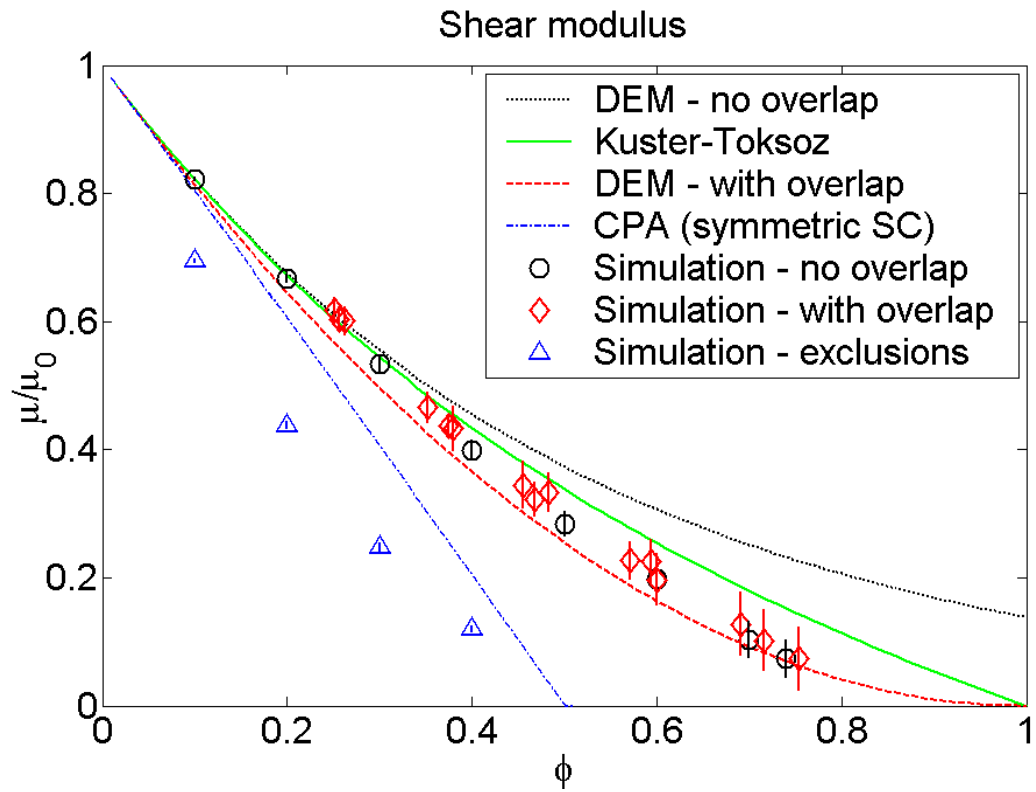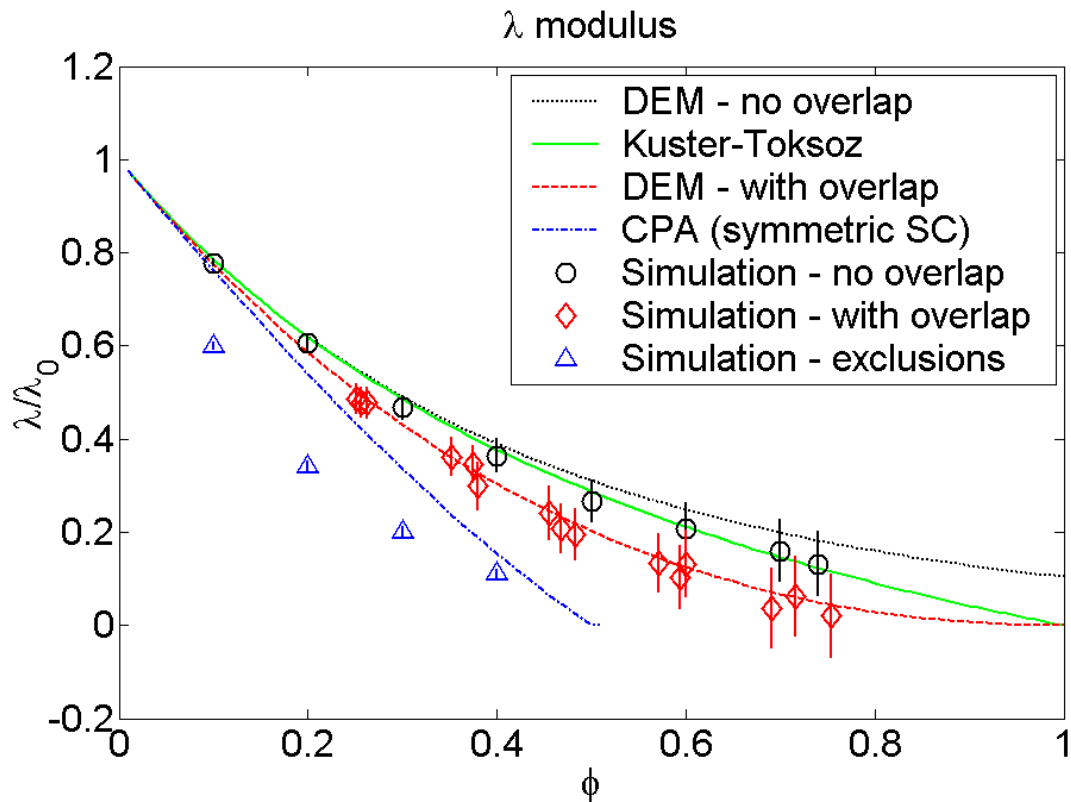

FIG. 7. The dependence of bulk modulus on porosity.

Shear modulus

FIG. 9. The dependence of shear modulus on porosity.

λ modulus

FIG. 9. The dependence of the λ modulus on porosity.
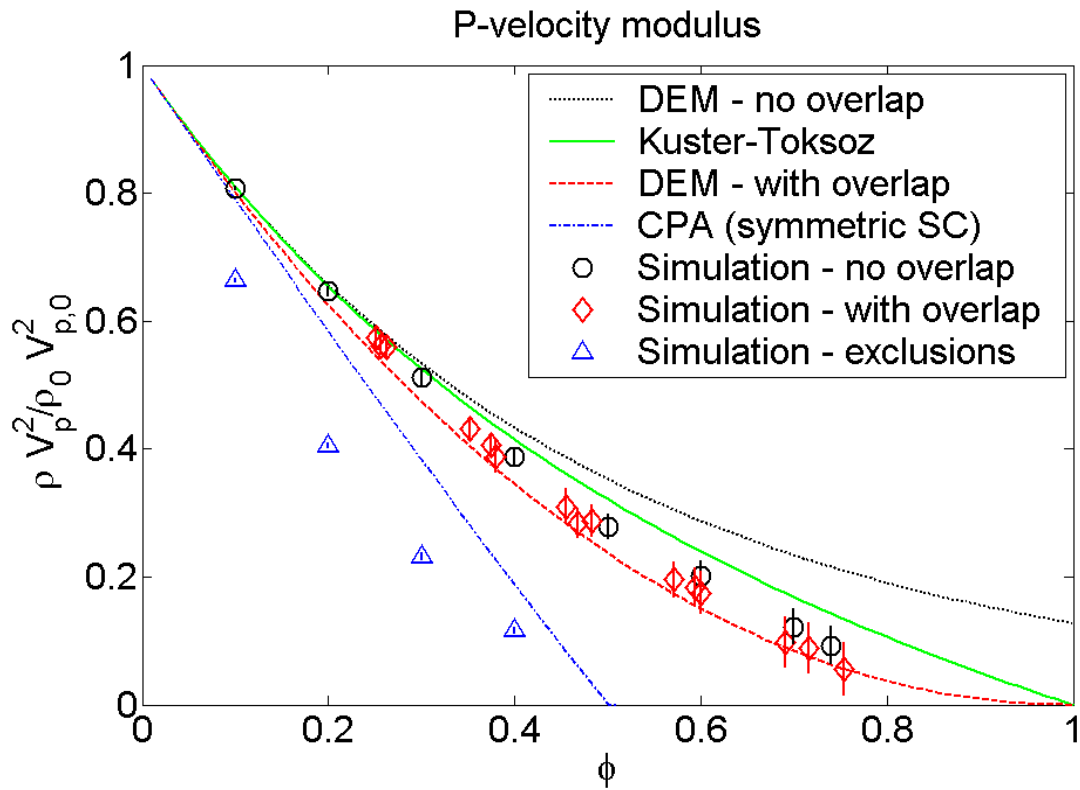
P-velocity modulus

FIG. 10. The dependence of the P-velocity modulus (or M) on porosity.
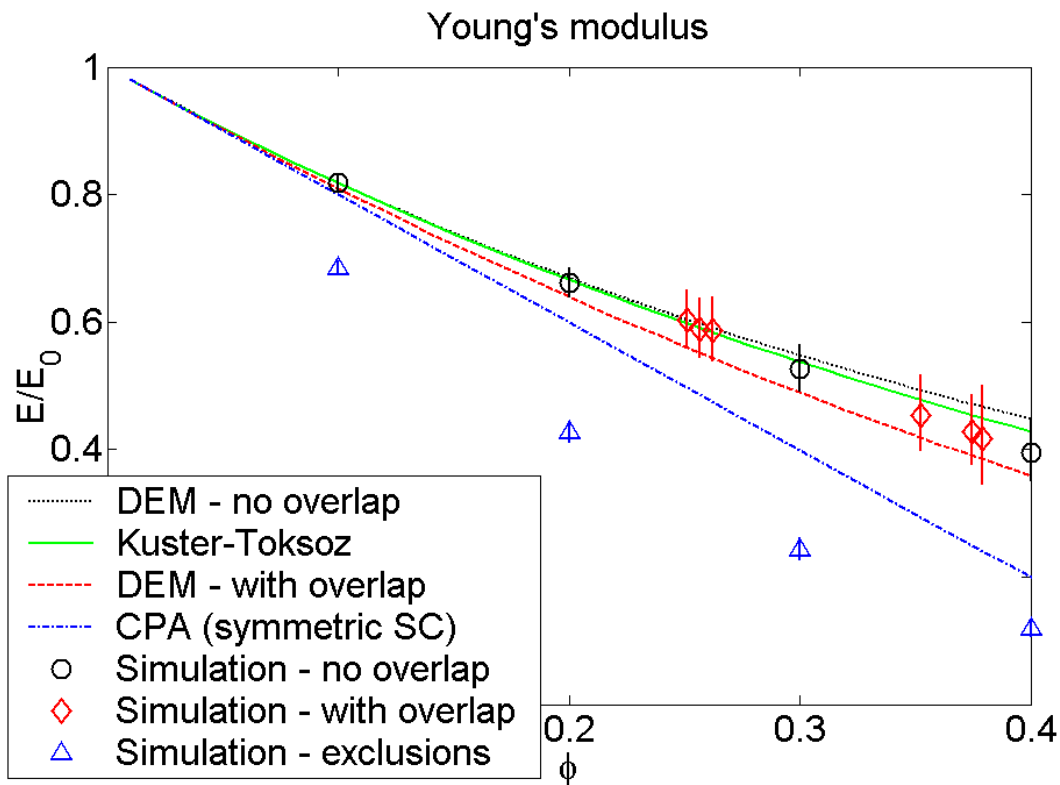
Young's modulus

FIG. 11. The dependence of Young's modulus on porosity.
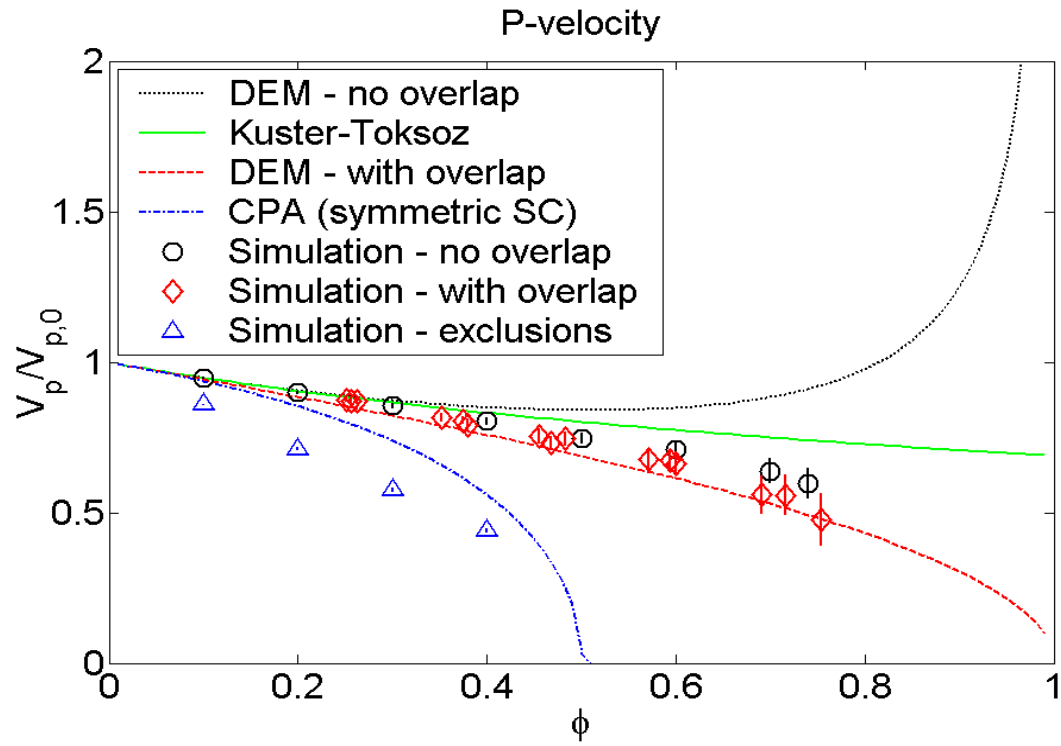
P-velocity

FIG. 12. The dependence of P-velocity on porosity.
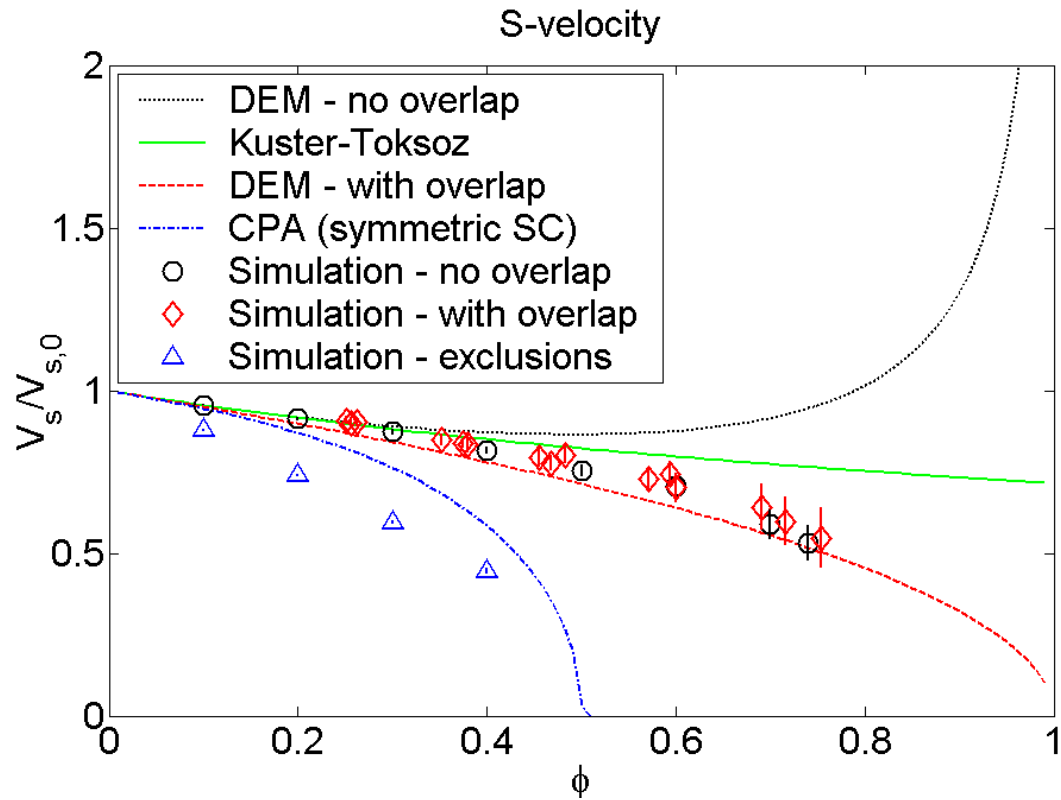
S-velocity

FIG. 13. The dependence of shear velocity on porosity.

The final derived quantity to present is the pore bulk modulus, K_P. This is defined in the present notation by the expression

$$\frac{\phi}{K_P} = \frac{1}{K} - \frac{1}{K_0}$$

(5)

or, rearranging,

$$\frac{K_P}{K_0} = \frac{(K/K_0)\phi}{1-(K/K_0)}.$$

(6)

Equation (5) is sometimes used to calculate the bulk modulus at some porosity, given the bulk modulus at another porosity, and assuming that the pore bulk modulus is independent of porosity. The simulations give us the opportunity to test this assumption, and Figure 14 below suggests that it is a poor assumption.
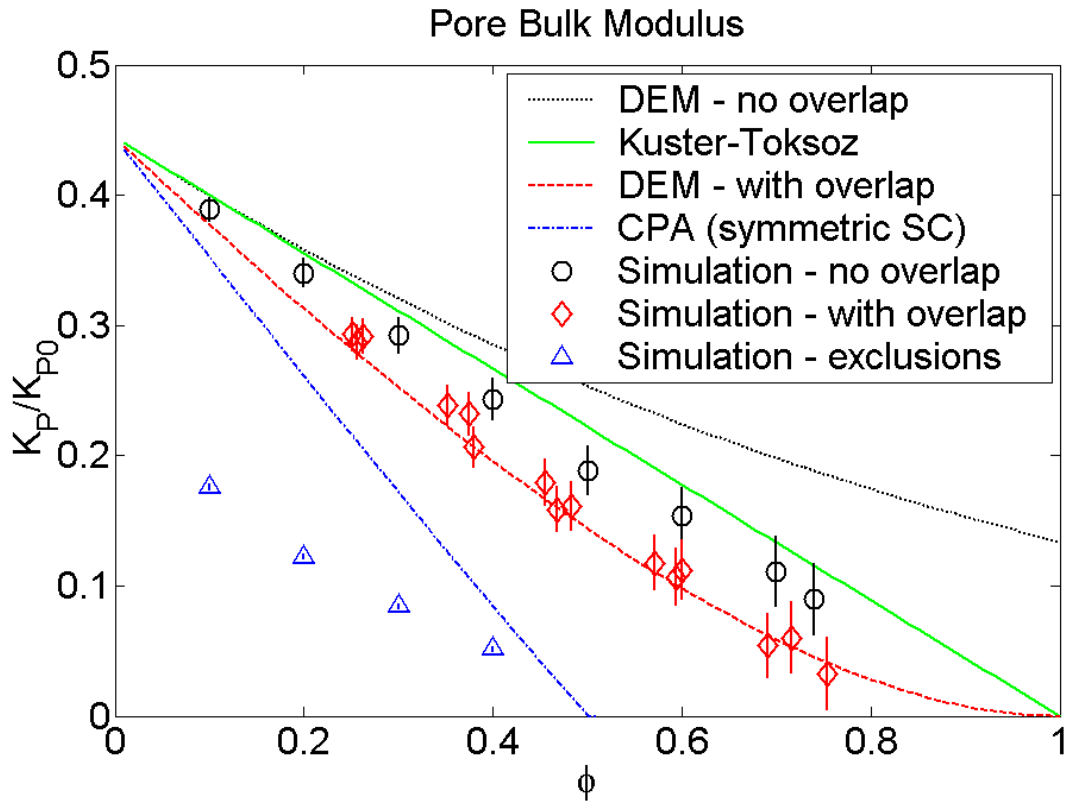

FIG. 14. The dependence of pore bulk modulus on porosity.

DISCUSSION

Focussing now on comparison with theory, the overlapping sphere sample appears to be best described by Norris' DEM theory. The shear modulus prediction is slightly low, but the bulk modulus prediction is excellent. This is reminiscent of the study by Berge *et al.* (1993) which showed that Norris' DEM was reasonably accurate in

predicting the bulk modulus of porous glass. However, porous glass contains non-overlapping pores, so the apparent agreement must be partly due to the imperfect modeling of glass pores. This serves to emphasize the key role of simulation studies in evaluating theory.

Next one notes that simulation exhibits behaviour similar to theory in that non-overlapping pores generally exhibit higher moduli than overlapping pores. However, it appears that Zimmerman's DEM, intended to represent non-overlapping pores, is not as accurate as the simpler Kuster-Toksöz model. One weakness of the Zimmerman DEM is that it does not vanish, even for $\phi = 1$, which is clearly unphysical. In fact, simulation results for non-overlapping spheres can only be carried out up to $\phi \approx .74$, which corresponds to the close packing of uniform spherical pores.

The CPA, which in principle treats both matrix and pores symmetrically, was shown by Berge *et al.* (1993) to be more descriptive of spherical exclusions than of spherical inclusions, and this is consistent with the results shown here. The agreement of the CPA is not as good with the present simulation though as with experimental results on fused glass beads. This is probably due to differences in pore shape, since the fused glass beads are non-overlapping. Indeed, at any fixed porosity, one can see a decrease in moduli attending a progression in pore shape. Non-overlapping spherical pores are the stiffest pores and have the highest moduli. Allowing spherical pores to overlap creates some non-spherical but still relatively rounded pores. The pores of non-overlapping spherical exclusion (not simulated here, but typified by fused glass beads) have more crack-like regions in each pore, and would have lower moduli yet (conceivably near the line representing the CPA theory). Finally, overlapping exclusions could readily create some very narrow, slit-like pores, which give rise to the smallest moduli. We will simulate non-overlapping exclusions in the future to verify this picture and compare with fused glass bead results.

CONCLUSIONS

Three-dimensional simulations are shown to be useful in assessing various theoretical approaches. While none of the considered methods are yet fully satisfactory, Norris' DEM is shown to be quite accurate for several properties of porous media with overlapping pores, and the theory of Kuster and Toksöz is reasonably accurate for non-overlapping pores.

REFERENCES

Allen, M.P., and Tildesley, D.J., 1987, Computer Simulation of Liquids, Oxford University Press.

Berge, P.A., Berryman, J.G., and Bonner, B.P., 1993, Influence of microstructure on rock elastic properties, Geophys. Res. Lett., 20, 2619-22.

Berryman, J.G., 1992, Single-scattering approximations for coefficients in Biot's equations of poroelasticity, J. Acoust. Soc. Am., 91, 551-571.

Chen, J., Thorpe, M. F., and Davis L. C., 1995, Elastic Properties of Rigid Fiber-Reinforced Composites, J. Appl. Phys., 77, 4349-4360.

Christiansson, H., and Helsing, J., 1996, Poisson's ratio of fiber-reinforced composites, J. Appl. Phys., 79, 7582-7585.

Day, A.R., Snyder, K.A., Garboczi, E.J., and Thorpe, M.F., 1992, The elastic moduli of a sheet containing circular holes, J. Mech. Phys. Solids, 40, 1031-1051.

Eischen, J.W., and Torquato, S., 1993, Determining Elastic Behavior of Composites by the Boundary Element Method, J. Appl. Phys., 74, 159.

Garboczi, E.J., and Day, A.R., 1995, An algorithm for computing the effective linear elastic properties of heterogeneous materials: Three-dimensional results for composites with equal phase Poisson ratios, J. Mech. Phys. Solids, 43, 1349-1362.

Gazis, D.C., Herman, R., and Wallis, R.F., 1960, Surface elastic waves in cubic crystals, Phys. Rev., 119, 533-544.

Hashin, Z., 1962, The elastic moduli of heterogeneous materials, ASME J. Appl. Mech., 29, 143-150 & 765-766.

Helsing, J., 1995, An integral equation method for elastostatics of periodic composites, J. Mech. Phys. Solids, 43, 815-828.

Krebes, E.S., 1987, Reflection and transmission at plane boundaries in nonwelded contact, J. Can. Soc. Expl. Geophys., 23, 66-72.

Kuster, G.T., and Toksöz, M.N., 1974, Velocity and attenuation of seismic waves in two-phase media, Geophysics, 39, 587-618.

Montroll, E.W., 1947, Dynamics of a square lattice, J. Chem. Phys., 15, 575-591.

Norris, A.N., 1985, A differential scheme for the effective moduli of composites, Mechanics of Materials, 4, 1-16

Paranjape, B.V., and Arimitsu, N., Krebes, E.S., 1987, Reflection and transmission of ultrasound from a planar interface, J. Appl. Phys., 61, 888-894.

Poutet, J., Manzoni, D., Hage-Chehade, F., Jacquin, C.J., Boutéca, M.J., Thovert, J.-F., Adler, P.M., 1996, The effective mechanical properties of random porous media, J. Mech. Phys. Solids, 44, 1587-1620.

Scales, J.A., 2000, private communication.

Snyder, K.A., Garboczi, E.J., and Day A.R., 1992, The elastic moduli of simple two-dimensional isotropic composites: Computer simulation and effective medium theory, J. Appl. Phys., 72, 5948-5955.

Walsh, J.B., Brace, W.F., England, A.W., 1965, Effect of Porosity on Compressibility of Glass, J. Am. Cer. Soc., 48, 605-608.

Zimmerman, R.W., 1984, The elastic moduli of a solid with spherical pores: New self-consistent method, International Journal of Rock Mechanics and Mining Science, 21, 339-343.

Zimmerman, R.W., 1991, Compressibility of Sandstones, Elsevier (chapter 4).